Inorg. Chem. **2007**, *46*, 6029–6037

Substituent Effect on Formation of Heterometallic Molecular Wheels: Synthesis, Crystal Structure, and Magnetic Properties

Zhong-Hai Ni,[†] Li-Fang Zhang,[†] Vassilis Tangoulis,*[,‡] Wolfgang Wernsdorfer,[§] Ai-Li Cui,[†] Osamu Sato,[||] and Hui-Zhong Kou*[,†]

Department of Chemistry, Tsinghua University, Beijing 100084, People's Republic of China, Department of Chemistry, University of Patras, 26500 Patras, Greece, Laboratoire Louis Néel-CNRS, 38042 Grenoble Cedex 9, France, and Institute for Materials Chemistry and Engineering, Kyushu University, 6-1 Kasuga-koen, Kasuga, Fukuoka 816-8580, Japan

Received March 20, 2007

The reaction of manganese(III) Schiff bases of the type salen^{2-} (*N*,*N*′-ethylenebis(salicylideneaminato)) with X-substituted (X = CH_3, Cl) pyridinecarboxamide dicyanoferrite(III) [Fe(X-bpb)$(CN)_2]^-$ gave rise to a series of cyanide-bridged Mn_6Fe_6 molecular wheels, $[Mn^{III}(salen)]_6[Fe^{III}(bpmb)(CN)_2]_6 \cdot 7H_2O$ (**1**), $[Mn(salen)]_6[Fe(bpClb)(CN)_2]_6 \cdot 4H_2O \cdot 2CH_3OH$ (**2**), $[Mn(salen)]_6[Fe(bpdmb)(CN)_2]_6 \cdot 10H_2O \cdot 5CH_3OH$ (**3**), $[Mn(5\text{-}Br(salpn))]_6[Fe(bpmb)(CN)_2]_6 \cdot 24H_2O \cdot 8CH_3CN$ (**4**), and $[Mn(5\text{-}Cl(salpn))]_6[Fe(bpmb)(CN)_2]_6 \cdot 25H_2O \cdot 5CH_3CN$ (**5**). Compared with $[Fe(bpb)(CN)_2]^-$, which always gives rise to 1D or polynuclear species when reacting with Mn(III) Schiff bases, the introduction of substituents (X) to the bpb^{2-} ligand has a driving force in formation of the novel wheel structure. Magnetic studies reveal that high-spin ground state $S = 15$ is present in the wheel compounds originated from the ferromagnetic Mn(III)–Fe(III) coupling. For the first time, the quantum Monte Carlo study has been used to modulate the magnetic susceptibility of the huge Mn_6Fe_6 metallomacrocycles, showing that the magnetic coupling constants J range from 3.0 to 8.0 K on the basis of the spin Hamiltonian $H = -J(\sum_{i,j} s_{Fei} S_{Mnj} + s_{Fe1} S_{Mn12})$. Hysteresis loops for **1** have been observed below 0.8 K, indicative of a single-molecule magnet with a blocking temperature (T_B) of 0.8 K. Molecular wheels **2**–**5** exhibit frequency dependence of alternating-current magnetic susceptibility under zero direct-current magnetic field, signifying the slow magnetization relaxation similar to that of **1**. Significantly, an unprecedented archlike Mn_2Fe_2 cluster, $[Mn(5\text{-}Cl(salpn))]_2[Fe(bpmb)(CN)_2]_2 \cdot 3H_2O \cdot CH_3CN$ (**6**), has been isolated as an intermediate of the Mn_6Fe_6 wheel **5**. Ferromagnetic Mn(III)–Fe(III) coupling results in a high-spin $S = 5$ ground state. Combination of the high-spin state and a negative magnetic anisotropy (D) results in the observation of slow magnetization relaxation in **6**.

Introduction

The design and synthesis of metallamacrocycles continue to attract a great deal of interest, some of which exhibit interesting physical properties that are related to their particular molecular structures.[1,2] Multifarious metallamacrocycles including metallacrowns,[2,3] metallacalixarenes,[4] metallahelicates,[5] metallacryptates,[6] metallacyclophanes,[7] molecular polygons, and molecular wheels as well as other cyclic structures[1,8−12] have been isolated by rational selection of building blocks and bridging groups,[1,11] or by using appropriate templating anions and cations.[7,12] However, the

* To whom correspondence should be addressed. E-mail: vtango@upatras.gr (V.T.), kouhz@mail.tsinghua.edu.cn (H.-Z.K.).
[†] Tsinghua University.
[‡] University of Patras.
[§] Laboratoire Louis Néel-CNRS.
[||] Kyushu University.

(1) (a) Leininger, S.; Olenyuk, B.; Stang, P. J. *Chem. Rev.* **2000**, *100*, 853−908. (b) Swiegers, G. F.; Malefetse, T. J. *Chem. Rev.* **2000**, *100*, 3483−3537. (c) Fujita, M.; Umemoto, K.; Yoshizawa, M.; Fujita, N.; Kusukawa, T.; Biradha, K. *Chem. Commun.* **2001**, 509−518.
(2) (a) Bodwin, J. J.; Cutland, A. D.; Malkani, R. G.; Pecoraro, V. L. *Coord. Chem. Rev.* **2001**, *216*−*217*, 489−512. (b) Pecoraro, V. L.; Bodwin, J. J.; Cutland, A. D. *J. Solid State Chem.* **2000**, *152*, 68−77.
(3) (a) Liu, S.-X.; Lin, S.; Lin, B.-Z.; Lin, C.-C.; Huang, J.-Q. *Angew. Chem., Int. Ed.* **2001**, *40*, 1084−1087. (b) John, R. P.; Lee, K.; Lah, M. S. *Chem. Commun.* **2004**, 2660−2661.
(4) (a) Rauter, H.; Hillgeris, E. C.; Erxleben, A.; Lippert, B. *J. Am. Chem. Soc.* **1994**, *116*, 616−624. (b) Rauterkus, M. J.; Krebs, B. *Angew. Chem., Int. Ed.* **2004**, *43*, 1300−1303.
(5) Johnson, J. A.; Kampf, J. W.; Pecoraro, V. L. *Angew. Chem., Int. Ed.* **2003**, *42*, 546−549.

10.1021/ic700528a CCC: $37.00
Published on Web 06/28/2007

Scheme 1. Structures of Building Blocks $[Fe^{III}(L)(CN)_2]^{-}$ [a] and $[Mn^{III}(Schiff\ base)]^{+}$ [b]

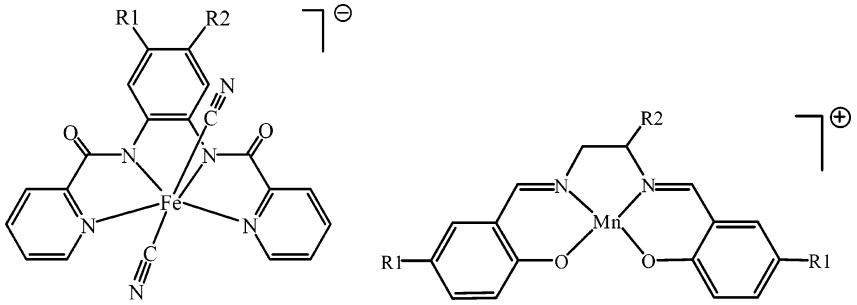

[a] L = bpb^{2-} (R1 = R2 = H), $bpmb^{2-}$ (R1 = H, R2 = CH_3), $bpClb^{2-}$ (R1 = H, R2 = Cl), $bpdmb^{2-}$ (R1 = R2 = CH_3). [b]Schiff base = $salen^{2-}$ (R1 = R2 = H), 5-Cl($salen^{2-}$) (R1 = Cl, R2 = H), 5-Br($salen^{2-}$) (R1 = Br, R2 = H), 5-Me($salen^{2-}$) (R1 = CH_3, R2 = H), 5-MeO($salen^{2-}$) (R1 = CH_3O, R2 = H), 5-Cl($salpn^{2-}$) (R1 = Cl, R2 = CH_3), 5-Br($salpn^{2-}$) (R1 = Br, R2 = CH_3).

generation of metallamacrocycles with desired structures and functionalities is still a substantial challenge.

It is worth noting that some metallamacrocycles have been recently recognized as a novel class of molecules known as single-molecule magnets (SMMs).[6a,8,13] SMMs present a molecular approach to a nanoscale magnet, and have been one of the hot topics in physics, chemistry, and materials science as well as molecular nanotechnology over the past decade.[8,13] SMMs not only exhibit classical magnet behaviors, but also offer the most appropriate medium for the study of quantum tunneling and slow relaxation of magnetization. More significantly, they can be potentially used in high-density data-storage technology, quantum computation, spin-based molecular electronics, or magnetic refrigeration.[13] To search for new SMMs with good magnetic performance and to improve the magnetic properties of the existing SMMs, a number of SMMs have been synthesized and characterized to date.[13] After a decade of research, it has been established that the magnetic behavior of an SMM is related to the spin ground state (S) and the axial magnetic anisotropy ($-D_{mol}$) of the molecule, which lead to the energy barrier (U) for reversing the spin orientations between microstates $+M_S$ and $-M_S$. Therefore, at a certain temperature (close to the blocking temperature T_B) the SMM should exhibit slow relaxation of magnetization with a half-life dependent on U. According to $U = S^2|D|$ for an integral spin or $U = (S^2 - 1/4)|D|$ for a half-integral spin, the magnetic properties of an SMM can be therefore improved by increasing S or $|D|$.[13]

Cyanide ligand (CN^-) can effectively transmit magnetic coupling between different metal centers. More importantly, the topological structures of metal−cyanide clusters and the nature of the metallic magnetic interactions can be easily controlled and anticipated.[14] This strategy has led to the successful preparation of a few cyanide-bridged SMMs with high-spin ground states and axial magnetic anisotropy.[15] To establish a new and more viable synthetic route to cyanide-bridged SMMs with new structural types, we focus on pyridinecarboxamide dicyanometalate building blocks *trans*-$[Fe(L)(CN)_2]^-$ and Schiff base Mn(III) complexes (Scheme 1), the latter possessing magnetic anisotropy that is important for SMMs.[15] The construction of large clusters consisting of Mn(III) and low-spin Fe(III) ions would possibly give new SMMs. To this end, we prepared a series of novel dodecanuclear $Mn^{III}_6Fe^{III}_6$ molecular wheels (**1**−**5**) as well as one new archlike $Mn^{III}_2Fe^{III}_2$ cluster (**6**), which is reported herein.

(6) (a) Zaleski, C. M.; Depperman, E. C.; Dendrinou-Samara, C.; Alexiou, M.; Kampf, J. W.; Kessissoglou, D. P.; Kirk, M. L.; Pecoraro, V. L. *J. Am. Chem. Soc.* **2005**, *127*, 12862−12872. (b) Dendrinou-Samara, C.; Alexiou, M.; Zaleski, C. M.; Kampf, J. W.; Kirk, M. L.; Kessissoglou, D. P.; Pecoraro, V. L. *Angew. Chem., Int. Ed.* **2003**, *42*, 3763−3766.

(7) Campos-Fernández, C. S.; Schottel, B. L.; Chifotides, H. T.; Bera, J. K.; Koomen, J. M.; Russell, D. H.; Dunbar, K. R. *J. Am. Chem. Soc.* **2005**, *127*, 12909−12923.

(8) (a) Tasiopoulos, A. J.; Vinslava, A.; Wernsdorfer, W.; Abboud, K. A.; Christou, G. *Angew. Chem., Int. Ed.* **2004**, *43*, 2117−2121. (b) Murugesu, M.; Raftery, J.; Wernsdorfer, W.; Christou, G.; Brechin, E. K. *Inorg. Chem.* **2004**, *43*, 4203−4209. (c) Rumberger, E. M.; Shah, S. J.; Beedle, C. C.; Zakharov, L. N.; Rheingold, A. L.; Hendrickson, D. N. *Inorg. Chem.* **2005**, *44*, 2742−2752. (d) Foguet-Albiol, D.; O'Brien, T. A.; Wernsdorfer, W.; Moulton, B.; Zaworotko, M. J.; Abboud, K. A.; Christou, G. *Angew. Chem., Int. Ed.* **2005**, *44*, 897−901. (e) Rumberger, E. M.; Zakharov, L. N.; Rheingold, A. L.; Hendrickson, D. N. *Inorg. Chem.* **2004**, *43*, 6531.

(9) (a) Caneschi, A.; Gatteschi, D.; Laugier, J.; Rey, P.; Sessoli, R.; Zanchini, C. *J. Am. Chem. Soc.* **1988**, *110*, 2795−2799. (b) Huang, X.-C.; Zhang, J.-P.; Chen, X.-M. *J. Am. Chem. Soc.* **2004**, *126*, 13218−13219. (c) Jones, L.; Batsanov, A.; Brechin, E.; Collison, D.; Helliwell, M.; Mallah, T.; McInnes, E.; Piligkos, S. *Angew. Chem., Int. Ed.* **2002**, *41*, 4318.

(10) (a) Taft, K. L.; Delfs, C. D.; Papaefthymiou, G. C.; Foner, S.; Gatteschi, D.; Lippard, S. J. *J. Am. Chem. Soc.* **1994**, *116*, 823−832. (b) Larsen, F. K.; Overgaard, J.; Parsons, S.; Rentschler, E.; Smith, A. A.; Timco, G. A.; Winpenny, R. E. P. *Angew. Chem., Int. Ed.* **2003**, *42*, 5978−5981. (c) Chang, C.-H.; Hwang, K. C.; Liu, C.-S.; Chi, Y.; Carty, A. J.; Scoles, L.; Peng, S.-M.; Lee, G.-H.; Reedijk, J. *Angew. Chem., Int. Ed.* **2001**, *40*, 4651−4653. (d) Roh, S. G.; Park, K.-M.; Park, G.-J.; Sakamoto, S.; Yamaguchi, K.; Kim, L. *Angew. Chem., Int. Ed.* **1999**, *38*, 637−641. (e) Kim, J.; Han, S.; Pokhodnya, K. I.; Migliori, J. M.; Miller, J. S. *Inorg. Chem.* **2005**, *44*, 6983−6988.

(11) (a) Oshio, H.; Onodera, H.; Ito, T. *Chem.−Eur. J.* **2003**, *9*, 3946−3950. b) Karada, F.; Schelter, E. J.; Prosvirin, A. V.; Bacsa, J.; Dunbar, K. R. *Chem. Commun.* **2005**, 1414−1416.

(12) (a) Heath, S. L.; Laye, R. H.; Muryn, C. A.; Lima, N.; Sessoli, R.; Shaw, R.; Teat, S. J.; Timco, G. A.; Winpenny, R. E. P. *Angew. Chem., Int. Ed.* **2004**, *43*, 6132−6135. (b) Bretonnière, Y.; Mazzanti, M.; Pécaut, J.; Olmstead, M. M. *J. Am. Chem. Soc.* **2002**, *124*, 9012−9013.

(13) See reviews: Bircher, R.; Chaboussant, G.; Dobe, C.; Güdel, H. U.; Ochsenbein, S. T.; Sieber, A.; Waldmann, O. *Adv. Funct. Mater.* **2006**, *16*, 209−220. Aromi, G.; Brechin, E. K. *Struct. Bonding* **2006**, *112*, 1−67. Long, J. R. *Chemistry of Nanostructured Materials*; World Scientific Publishing: Hong Kong, 2003; pp 291−315. Sessoli, R.; Gatteschi, D. *Angew. Chem., Int. Ed.* **2003**, *42*, 268−297. Brechin, E. K. *Chem. Commun.* **2005**, 5141−5153.

(14) Beltran, L. M. C.; Long, J. R. *Acc. Chem. Res.* **2005**, *38*, 325−334.

(15) Rebilly, J.-N.; Mallah, T. *Struct. Bonding* **2006**, *122*, 103−131. Lescouëzec, R.; Toma, L. M.; Vaissermann, J.; Verdaguer, M.; Delgado, F. S.; Ruiz-Pérez, C.; Lloret, F.; Julve, M. *Coord. Chem. Rev.* **2005**, *249*, 2691−2729.

Table 1. Crystallographic Data for Complexes **2**−**6**

	2	**3**	**4**	**5**	**6**
empirical formula	$Fe_6Mn_6C_{218}H_{162}Cl_6N_{48}O_{30}$	$Fe_6Mn_6C_{233}H_{220}N_{48}O_{39}$	$Fe_6Mn_6C_{244}H_{234}Br_{12}N_{56}O_{48}$	$Fe_6Mn_6C_{238}H_{227}Cl_{12}N_{53}O_{49}$	$Fe_2Mn_2C_{78}H_{66}Cl_4N_{17}O_{11}$
fw	4811.40	4981.32	6342.53	5703.84	1780.86
T, K	113	173	123	113	293
cryst syst	triclinic	triclinic	hexagonal	hexagonal	triclinic
space group	$P\bar{1}$	$P\bar{1}$	$P\bar{3}$	$P\bar{3}$	$P\bar{1}$
a, Å	13.712(3)	13.718(3)	25.073(4)	25.009(5)	13.248(13)
b, Å	20.604(6)	21.098(4)	25.073(4)	25.009(5)	18.659(18)
c, Å	20.674(5)	21.117(4)	12.7482(18)	12.512(2)	19.04(2)
α, deg	81.703(10)	78.69(3)	90	90	115.82(5)
β, deg	76.112(9)	77.61(3)	90	90	106.82(5)
γ, deg	86.273(10)	87.18(3)	120	120	91.45(4)
V, Å^3	5608(2)	5853(2)	6940(2)	6777(2)	3992(7)
Z	1	1	1	1	2
ρ_{calcd}, g cm^{-3}	1.425	1.413	1.466	1.397	1.481
μ, mm^{-1}	0.850	0.734	2.367	0.778	0.870
no. of obsd data [$I > 2(I)$]	16404	13731	7597	7200	12034
GOF	1.076	1.049	0.866	1.057	1.033
R1 [$I > 2\sigma(I)$]	0.0871	0.0924	0.0936	0.0761	0.0532
wR2 (all data)	0.2292	0.2729	0.2323	0.1910	0.1415

Table 2. Comparison of Bond Distances (Å) and Bond Angles (deg) for Complexes **1**−**5**

	1	**2**	**3**	**4**	**5**
Mn−N_{cyano}	2.258(5)−2.354(4)	2.250(4)−2.320(4)	2.281(5)−2.370(5)	2.234(7)−2.256(6)	2.236(4)−2.259(4)
Mn−N_{salen}	1.966(5)−1.984(4)	1.983(5)−1.993(5)	1.973(6)−1.986(6)	1.989(7)−2.006(7)	1.995(4)−2.004(4)
Mn−O_{salen}	1.835(3)−1.879(3)	1.863(4)−1.887(4)	1.868(4)−1.883(4)	1.878(6)−1.880(5)	1.880(3)−1.884(3)
Fe−C	1.941(6)−1.984(6)	1.934(6)−1.970(6)	1.935(7)−1.970(6)	1.934(9)−1.958(8)	1.944(5)−1.958(4)
Fe−$N_{pyridine}$	1.965(5)−2.019(6)	1.968(5)−2.027(6)	1.970(5)−2.001(5)	1.980(8)−1.997(7)	1.991(5)−1.993(4)
Fe−N_{amide}	1.855(5)−1.897(5)	1.874(8)−1.913(7)	1.874(5)−1.909(7)	1.883(8)−1.894(7)	1.883(4)−1.915(4)
Mn−NC	140.8(4)−163.3(5)	138.4(4)−161.4(6)	141.6(5)−170.2(6)	147.7(7)−158.2(6)	145.8(4)−158.4(3)
Fe−CN	168.5(5)−178.2(5)	168.8(5)−177.9(6)	170.4(6)−176.7(6)	175.5(7)−175.8(7)	175.1(4)−176.2(4)
N_{cyano}−Mn−N_{cyano}	172.1(2)−174.6(2)	174.5(2)−175.2(2)	170.0(2)−173.5(2)	174.8(3)	175.24(16)

Results and Discussion

Synthesis. The precursor K[Fe(L)$(CN)_2$] contains two *trans*-cyanide groups with pyridinecarboxamide ligand L at its equatorial plane. Another reactant, *trans*-[Mn(Schiff base)]$^+$, has two available axial sites for coordination by cyanide nitrogen atoms. Moreover, [Mn(Schiff base)]$^+$ has one positive charge, while K[Fe(L)$(CN)_2$] possesses one negative charge. Therefore, in principle, the combination of K[Fe(L)$(CN)_2$] and [Mn(Schiff base)]ClO_4 building blocks should yield low-dimensional complexes such as 1D chain complexes or linear polynuclear clusters. However, an unexpected construction of metallamacrocycle compound **1** occurs when [Fe(bpmb)$(CN)_2]^-$ is used for the synthesis.[16] The methyl group in the bpmb^{2-} ligand has been assumed to be responsible for the metallamacrocycle formation. To gain more evidence to support this supposition, we tried other substitution groups, for instance chloro. Therefore, we synthesized three cyanide-containing building blocks, K[Fe(L)$(CN)_2$] (L = bpmb^{2-}, bpClb^{2-}, or bpdmb^{2-}). As expected, four more dodecanuclear molecular-gearwheel-like compounds (**2**−**5**) with a crystal structure similar to that of compound **1** have been obtained. In addition, we successfully separated a tetranuclear arch-shaped complex (**6**) in the preparation of the wheel complex **5**. These results support our proposition that some small substituted groups, such as methyl, chloro, or dimethyl in bpb^{2-}, favor the formation of molecular-wheel-like compounds.

X-ray diffraction (XRD) spectra of complexes **2**−**6** have been measured at room temperature and are in good agreement with the calculated patterns derived from the single-crystal diffraction data. The purity of the samples is also verified by the elemental analyses.

Table 3. Selected Bond Distances (Å) and Bond Angles (deg) for Complex **6**

Mn(1)−N(1)	2.349(3)	Mn(1)−N(3)	2.315(3)
Mn(1)−N(14)	1.984(3)	Mn(1)−O(5)	1.863(3)
Mn(1)−N(13)	1.987(3)	Mn(1)−O(6)	1.863(3)
Mn(2)−N(16)	1.981(3)	Mn(2)−N(4)	2.280(4)
Mn(2)−N(15)	1.982(3)	Mn(2)−O(1w)	2.259(3)
Mn(2)−O(8)	1.886(3)	Mn(2)−O(7)	1.867(3)
Fe(1)−C(1)	1.974(4)	Fe(1)−C(2)	1.955(4)
Fe(2)−C(4)	1.962(4)	Fe(2)−C(3)	1.974(4)
Mn(1)−N(1)−C(1)	147.2(3)	Mn(1)−N(3)−C(3)	147.2(2)
Mn(2)−N(4)−C(4)	155.4(3)	Fe(1)−C(1)−N(1)	173.4(3)
Fe(1)−C(2)−N(2)	176.2(3)	Fe(2)−C(3)−N(3)	176.1(3)
Fe(2)−C(4)−N(4)	172.2(3)	N(2)−Mn(1)−N(3)	171.93(9)
N(4)−Mn(2)−O(1w)	173.91(10)		

All complexes are moderately soluble in polar solvents, MeCN, MeOH, or DMF.

Structural Descriptions. The structure of compound **1** has been briefly reported elsewhere.[16] Crystal data and structure refinement details for compounds **2**−**6** are listed in Table 1. Important structural parameters of complexes **1**−**6** are collected in Tables 2 and 3. The structural diagrams of complexes **3**, **5**, and **6** are shown in Figures 1−4, while figures showing the structures of the other complexes are given in the Supporting Information (Figures S1−S7).

X-ray structural analyses reveal that complexes **1**−**3** are isostructural, and all crystallize in triclinic space group $P\bar{1}$. The core of complexes **1**−**3** consists of a neutral [Mn(salen)]$_6$[Fe(L)$(CN)_2]_6$ (L = bpmb^{2-}, bpClb^{2-}, or bpdmb^{2-}) framework in which 6 Mn(III) and 6 Fe(III) ions are alternately bridged by 12 cyanide groups, leading to a

(16) Ni, Z.-H.; Kou, H.-Z.; Zhang, L.-F.; Ge, C.; Cui, A.-L.; Wang, R.-J.; Li, Y.; Sato, O. *Angew. Chem., Ed. Int.* **2005**, *44*, 7742−7745.

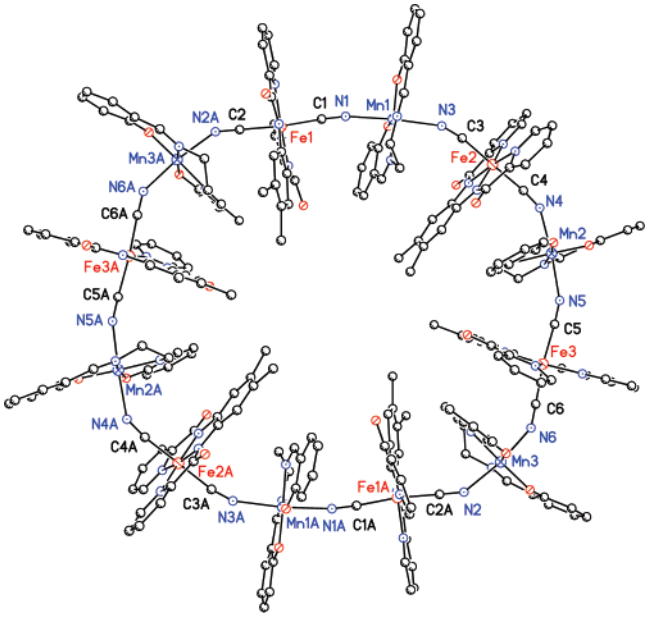

Figure 1. Crystal structure of the dodecanuclear molecular wheel **3**.

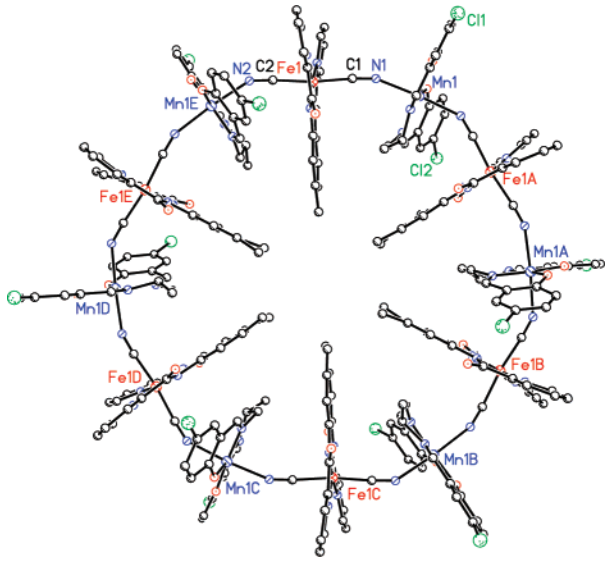

Figure 2. Dodecanuclear structure of complex **5** with a regular cyclic structure.

centrosymmetrical 36-membered elliptical macrocycle (Figures 1 and S1−S3). The iron(III) ions in complexes **1**−**3** are hexacoordinated by two pyridine nitrogen and two amide nitrogen atoms from deprotonated pyridinecarboxamide ligand $bpmb^{2-}$, $bpClb^{2-}$, or $bpdmb^{2-}$ located in the equatorial plane and two cyanide carbon atoms at two *trans* sites, giving a slightly distorted octahedral geometry. Each manganese ion in complexes **1**−**3** is coordinated with two cyanide nitrogen atoms at *trans* positions and two imine nitrogen as well as two phenoxo oxygen atoms from the $salen^{2-}$ ligand in the equatorial plane, yielding an elongated octahedral MnN_4O_2 coordination geometry. The Mn−N≡C bond angles (138.4(4)−163.3(5)°) deviate significantly from linearity with the exception of Mn(1)−N(1)−C(1) (170.2(6)°) in **3**. The average Mn−N≡C bond angles are very similar, being 151.5(4)° for **1**, 151.3(5)° for **2**, and 153.5(5)° for **3**. The metal−metal distances bridged by cyanide groups are distributed within the ranges 5.089−5.341 Å (**1**), 5.041−5.313 Å (**2**), and 5.104−5.371 Å (**3**). The shortest intermolecular metal−metal separations are 6.808 Å (**1**), 6.732 Å (**2**), and 6.932 Å (**3**).

It is worth pointing out that the longest intramolecular metal−metal distances that correspond to the major axis of the ellipse are 21.778 Å (Mn(1)−Mn(1)$^{\#}$, symmetry operation $-x + 3, -y + 1, -z + 1$), 21.818 Å (Fe(3)−Fe(3)$^{\#}$, symmetry operation $-x + 2, -y, -z + 1$), and 21.261 Å (Mn(2)−Mn(2)$^{\#}$, symmetry operation $-x + 1, -y, -z + 1$) for complexes **1**, **2**, and **3**, respectively. The metal−metal separations near the minor axis of the ellipse are 17.728 Å (Fe(3)−Fe(3)$^{\#}$) for **1**, 17.659 Å (Fe(1)−Fe(1)$^{\#}$) for **2**, and 17.659 Å (Fe(1)−Fe(1)$^{\#}$) for **3**. In addition, there exist manifest intramolecular and intermolecular $\pi-\pi$ interactions as well as O−H−O hydrogen bonds between amide oxygen atoms and free water molecules in three dimensions.

Compounds **4** and **5** are isostructural and crystallize in a highly symmetrical hexagonal space group, $P\bar{3}$ (Figure 2). Unlike complexes **1**−**3** consisting of Mn_3Fe_3 independent units, complexes **4** and **5** are formed through a 6-fold rotation axis symmetry operation of the Mn(1)Fe(1) independent unit. Therefore, the gearwheel-like molecular structures of complexes **4** and **5** are close to regular circles compared with those of complexes **1**−**3**.

The coordination environment of Fe(III) and Mn(III) in **4** and **5** resembles that in **1**−**3**. The two Mn−N≡C linkages are in a bent fashion, viz., Mn(1)−N(1)−C(1) = 147.7(7)° and Mn(1)$^{\#2}$−N(2)−C(2) = 158.2(6)° for **4** and Mn(1)−N(1)−C(1) = 158.4(3)° and Mn(1)$^{\#2}$−N(2)−C(2) = 145.8(4)° for **5**. The shortest intermolecular metal−metal separations are 6.450 Å (**4**) and 6.425 Å (**5**). The metal−metal separations between two opposite metal ions in the wheels are 19.455 and 20.305 Å (**4**) and 19.431 and 20.253 Å (**5**) for two opposite Fe(III) and Mn(III) ions, respectively, showing that complexes **1**−**6** are the largest molecular wheels among cyanide-bridged 3d complexes.

It is interesting to note that a rare columnar icositetranuclear water cluster has been found between two adjacent molecules (Figure 3). The water cluster can be described as a H-bonded double layer with O−O contacts ranging from 2.7 to 2.9 Å. The water cluster is not discrete and is further linked to 12 amido oxygen atoms (O(1) and O(2) and their symmetrical equivalents) of the $bpmb^{2-}$ ligands, giving rise to an infinite supramolecular structure (Figure S6).

Compound **6** possesses an arch-shaped neutral $Mn^{III}_2Fe^{III}_2$ tetranuclear cluster, as shown in Figure 4. The axial positions of Mn(1) are occupied by two cyanide nitrogen atoms with $Mn-N_{cyano}$ bond distances of 2.349(3) Å (Mn(1)−N(1)) and 2.315(3) Å (Mn(1)−N(3)), yielding a MnN_4O_2 coordination environment. Another Mn(III) ion (Mn(2)) is axially coordinated by one cyanide nitrogen atom (Mn(2)−N(4) = 2.280(4) Å) and one water oxygen atom (Mn(2)−O(1W) = 2.259(3) Å), resulting in a MnN_3O_3 coordination geometry. The Mn−N≡C bond angles in **6** range from 147.2(3)° to 155.4(3)°, slightly smaller than those of complexes **1**−**5**. Interestingly, two Mn_2Fe_2 molecules are linked together by hydrogen bonds between the nonbridging cyanide nitrogen

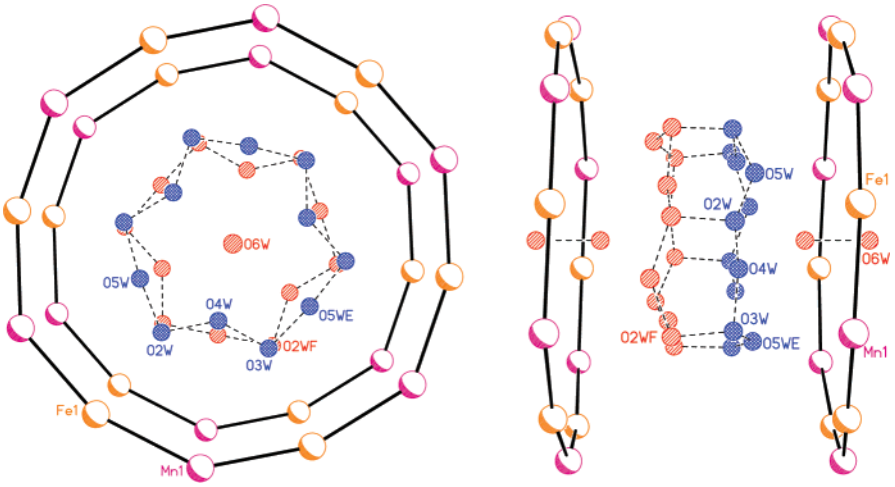

Figure 3. Top (left) and side (right) views of an icositetranuclear water cluster situated between two adjacent molecular wheels in **5** (purple, Mn; orange, Fe; red and blue, O). Different colors have been used to highlight the double-layered disposition of the H_2O molecules.

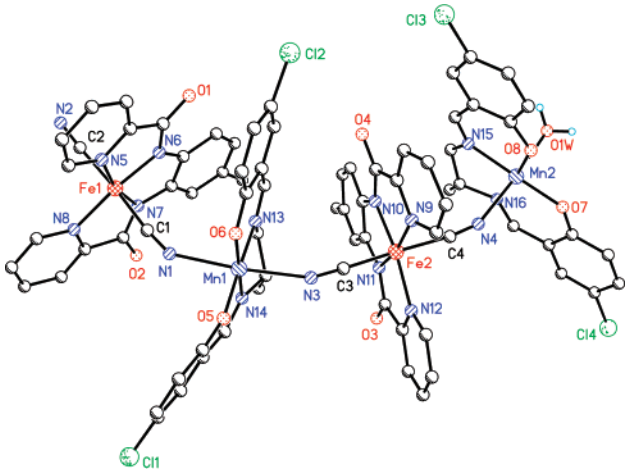

Figure 4. Tetranuclear archlike structure and 1D supramolecular structure of **6**.

atoms and the coordinated water molecules, forming elliptical $[Mn_2Fe_2]_2$ cyclic structures (Figure S7). The dimeric cycles are connected further by hydrogen bonds between coordinated water molecules and protonated phenoxo oxygen atoms, yielding one-dimensional supramolecular structures.

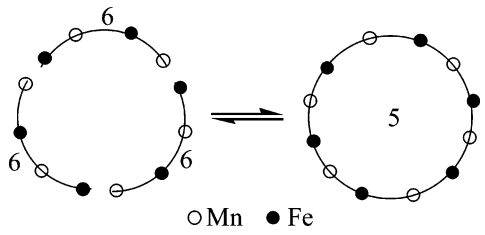

Isolation of the Mn_2Fe_2 intermediate suggests that the initial product is the tetranuclear species in the solution, which is similar in solubility to the wheel complex **5**. There is a thermodynamic equilibrium of 3(**6**) ⇌ **5**; therefore, both can be separated. Moreover, the presence of the archlike tetranuclear species **6** indicates that the inclusion of a substituent in the bpb^{2-} ligand is of help to the formation of cyclic molecules because we have found that no such archlike species have been isolated by using $[M(bpb)(CN)_2]^-$ (M = Fe, Co, Cr).

Magnetic Properties of Molecular Wheels 1−5. The variable-temperature magnetic susceptibilities of complexes **2**−**5** have been measured under an external magnetic field of 1000 G. Figure 5 shows the $\chi_m T$ vs T plots for **1**−**5**. The $\chi_m T$ values for complexes **1**−**5** in the 300 K range from 20.10 to 20.65 emu K mol^{-1}, consistent with the spin-only value of 20.25 emu K mol^{-1} for the uncoupled six high-spin Mn(III) atoms ($S = 2$) and six low-spin Fe(III) atoms ($S = 1/2$) based on $g = 2.00$. As temperature is decreased, the $\chi_m T$ values gradually increase and amount to 29.52 (5 K), 59.15 (2 K), 79.03 (2 K), 33.15 (5 K), and 26.73 (5 K) emu K mol^{-1} for complexes **1**, **2**, **3**, **4**, and **5**, respectively. These results suggest the presence of overall ferromagnetic interactions in complexes **1**−**5**.

To evaluate the strength of Mn(III)−Fe(III) magnetic coupling (J), quantum Monte Carlo (QMC) simulations were carried out based on the Hamiltonian

$$H = -J(\sum_{i,j} s_{Fei} S_{Mnj} + s_{Fe1} S_{Mn12}) \text{ (}i\text{, odd; }j\text{, even)} \quad (1)$$

on the assumption that all adjacent Mn(III)−Fe(III) magnetic exchange pathways are identical for simplicity. The reason for the use of Monte Carlo techniques is the large dimension of Hilbert's space (10^6), which excludes any other diagonalization technique. The final results of the simulations are shown as lines in the same figures. The simulations are verified in the temperature range 20−300 K, while in the low-temperature range the effect of interwheel magnetic interactions along with the zero-field splitting of the Mn(III) ions plays an important role. Due to the obvious difficulties concerning the diagonalization of the above Hamiltonian, it was not possible to include the zero-field splitting and/or the mean-field correction term. The simulation results are $J = 4.4(1)$ K and $g = 2.00(1)$ for **1**, $J = 6.5(1)$ K and $g = 1.98(1)$ for **2**, $J = 8.0(1)$ K and $g = 1.98(1)$ for **3**, $J = 4.4(1)$ K and $g = 2.05(1)$ for **4**, and $J = 3.0(1)$ K and $g = 2.01(1)$ for **5**. The fits are satisfactory with the agreement factors $R = (\Sigma(\chi_{calcd} - \chi_{obsd})^2)/\Sigma\chi_{obsd}^2 = 3 \times 10^{-5}$ for five complexes. The magnetic coupling constants range from 3.0(1) to 8.0(1) K, similar to those in cyanide-

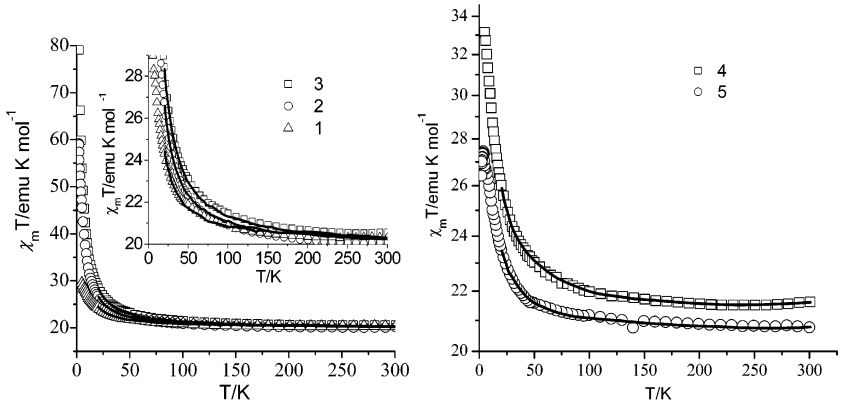

Figure 5. Temperature dependence of $\chi_M T$ for **1**−**5**. Inset: enlarged view. The solid lines represent the QMC simulations (20−300 K) according to the theoretical model discussed in the text.

bridged Mn(III)−Fe(III) complexes.[17] Alternatively, the alternating-spin chain model was used to fit the magnetic susceptibility curve based on the Hamiltonian $H = -J\sum_{i=0}^{N} S_i S_{i+1}$. The following equation (per MnFe) has been derived:

$$\chi_m = \frac{2N\beta^2}{3kT}\left[M^2\frac{1+P}{1-P} + (\delta M)^2\frac{1-P}{1+P}\right]$$

where $P = \coth(J_{eff}/kT) - kT/J_{eff}$, $M = [g_M[S_{Mn}(S_{Mn}+1)]^{1/2} + g_{Fe}[S_{Fe}(S_{Fe}+1)]^{1/2}]/2$, $\delta M = (g_{Mn}[S_{Mn}(S_{Mn}+1)]^{1/2} - g_{Fe}[S_{Fe}(S_{Fe}+1)]^{1/2})/2$, and $J_{eff} = J[S_{Mn}(S_{Mn}+1)S_{Fe}(S_{Fe}+1)]^{1/2}$.[18] To take into account the effects (e.g., zfs and intermolecular magnetic coupling) other than the intramolecular magnetic coupling, the mean-field approximation has been employed, giving the molar magnetic susceptibility (per Mn_6Fe_6) expression in the form $\chi_{mol/Mn_6Fe_6} = 6[\chi_m/(1 - 2zJ'\chi_m/Ng^2\beta^2)]$. One g value was used for simplification. The fitting results are $J = 6.8(2)$ cm^{-1}, $g = 1.99(1)$, $zJ' = -0.73(3)$ cm^{-1}, and $R = (\sum(\chi_{calcd} - \chi_{obsd})^2)/\sum\chi_{obsd}^2 = 5.5 \times 10^{-6}$ for **1**, $J = 6.92(8)$ cm^{-1}, $g = 1.97(1)$, $zJ' = -0.45(1)$ cm^{-1}, and $R = 7.3 \times 10^{-7}$ for **2**, $J = 7.09(8)$ cm^{-1}, $g = 1.99(1)$, $zJ' = -0.39(1)$, and $R = 4.6 \times 10^{-7}$ cm^{-1} for **3**, $J = 5.4(2)$ cm^{-1}, $g = 2.04(1)$, $zJ' = -0.46(4)$ cm^{-1}, and $R = 9.5 \times 10^{-7}$ for **4**, and $J = 1.86(2)$ cm^{-1}, $g = 2.02(1)$, $zJ' = 0$ cm^{-1}, and $R = 8.1 \times 10^{-6}$ for **5** (Figure S9, Supporting Information). It should be pointed out that the calculations are rough because of the employment of one J value for complicated examples. The J values may be close to the average values of the different kinds of magnetic coupling pathways related to different C≡N−Mn bond angles. Therefore, magentostructural correlation cannot be derived at the present stage for such complicated cases.

To determine the spin ground state values and the sign of the zero-field splitting (D) in these complexes, the magnetization measurements have been performed in the range 2−4 K and at an external magnetic filed of 10−50 kG. The curves of reduced magnetization ($M/N\mu_B$) versus H/T show that the isofield lines do not superimpose (Figures S9 and S10, Supporting Information), suggesting significant magnetic anisotropy (zero-field splitting) in the ground state. Given that the ground state is $S = 15$ and there is no population of excited spin state at low temperatures, the data were fit according to the following Hamiltonian:

$$H = g_{\parallel}\beta H_z S_z + g_{\perp}\beta(H_x S_x + H_y S_y) + SDS - zJ'\langle S_z\rangle S_z \qquad (2)$$

where the addition of the intermolecular interaction term $zJ'\langle S_z\rangle S_z$ is considered to be important for the fitting procedure.[19] The zfs D values are in a small range of −0.10(1) to −0.15(1) cm^{-1}. The fitting results (Figures S10 and S11, Supporting Information) were not satisfactory possibly because of the crude approximation of an isolated ground state. Nevertheless, in all cases, it seems that there is an important intermolecular contribution. Further magnetic measurements were carried out to verify their possible SMM character.

It is recognized that one of the most important characteristics of SMMs is the observation of a frequency-dependent out-of-phase (χ_m'') ac susceptibility signal. Thus, ac magnetic susceptibility measurements for complexes **1**−**5** were performed in a 3 G ac field oscillating at 111−9999 Hz, with a zero dc magnetic field, on the polycrystalline samples (Figures S12 and S13, Supporting Information). Indeed, complexes **1**−**5** all exhibit obvious frequency-dependent χ_m'' signals at $T < 3$ K, suggesting the presence of slow relaxation of magnetization.

To further confirm whether these wheel-like complexes behave as SMMs, single-crystal hysteresis loops and relaxation measurements for complex **1** were performed on a

(17) (a) Ni, W.-W.; Ni, Z.-H.; Cui, A.-L.; Liang, X.; Kou, H.-Z. *Inorg. Chem.* **2007**, *46*, 22−33. (b) Si, S.-F.; Tang, J.-K.; Liu, Z.-Q.; Liao, D.-Z.; Jiang, Z.-H.; Yan, S.-P.; Cheng, P. *Inorg. Chem. Commun.* **2003**, *6*, 1109−1112. (c) Miyasaka, H.; Clérac, R.; Mizushima, K.; Sugiura, K.; Yamashita, M.; Wernsdorfer, W.; Coulon, C. *Inorg. Chem.* **2003**, *42*, 8203−8213. (d) Miyasaka, H.; Nezu, T.; Sugimoto, K.; Sugiura, K.; Yamashita, M.; Clérac, R. *Chem.—Eur. J.* **2005**, *11*, 1592−1602. (e) Miyasaka, H.; Takahashi, H.; Madanbashi, T.; Sugiura, K.; Clérac, R.; Nojiri, H. *Inorg. Chem.* **2005**, *44*, 5969−5971. (f) Miyasaka, H.; Ieda, H.; Matsumoto, N.; Re, N.; Crescenzi, R.; Floriani, C. *Inorg. Chem.* **1998**, *37*, 255−263. (g) Choi, H. J.; Sokol, J. J.; Long, J. R. *Inorg. Chem.* **2004**, *43*, 1606−1608.

(18) Drillon, M.; Coronado, E.; Beltran, D.; Georges, R. *Chem. Phys.* **1983**, *79*, 449. This method is valid for pure classical spins, and the approximation for the present systems should be considered because of the presence of quantum spin $S_{Fe} = 1/2$. See: Kahn, O. *Molecular Magnetism*; Wieley-VCH Inc.: New York, 1993; pp 273−274.

(19) Different fitting procedures were carried out without using the intermolecular interaction term and/or the rhombic E term ($\lambda = E/D$). The fitting results were unrealistic, making the addition of these terms important.

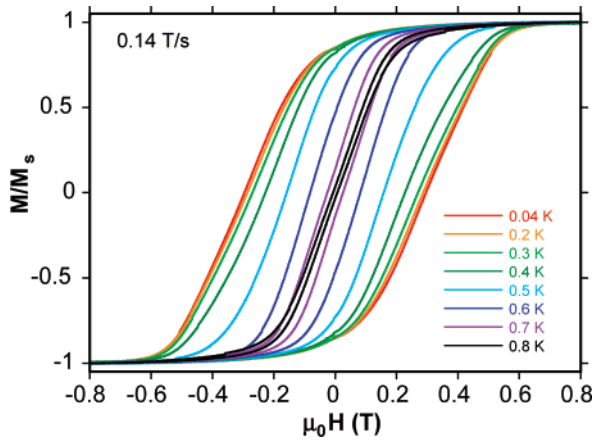

Figure 6. Hysteresis loop for complex **1** at different temperatures measured at a scan magnetic field speed of 0.14 T s^{-1}.

micro-SQUID magnetometer.[20] In the easy-axis direction, the magnetization exhibits a rapid saturation and hysteresis loops of classical magnet behaviors below 0.8 K (Figure 6). Moreover, the hysteresis loops are strongly dependent on the field sweep rate even at the lowest accessible temperature 0.04 K (Figure S14, Supporting Information). The coercivities of hysteresis loops were strongly temperature and time dependent, increasing with decreasing temperature and with increasing field sweep rate, as expected for an SMM. Below 0.2 K, the coercive field becomes temperature independent (Figure 6), signifying quantum tunneling of magnetization (QTM) between $M_S = +15$ and $M_S = -15$.[21] The blocking temperature (T_B) is about 0.8 K for **1**, above which hysteresis loops disappear. The hysteresis loop for **1** does not show the steplike features that are indicative of resonant QTM between the energy states of the molecules. The absence of QTM steps can be rationalized as being the relatively manifested intermolecular interactions (herein mainly $\pi-\pi$ stacking and hydrogen bonds between the adjacent wheels) which account for the broadening of the steps.[20] In addition, the distribution of molecular environments resulted from disordered lattice solvent molecules and ligand disorder, which usually leads to the distribution of magnetization relaxation barriers, and thus, broadening effects smear the steps out because the magnetic properties of SMMs are very sensitive to such relatively small variations in local environments.[8a] It is worth noting that this tendency of hysteresis loops showing no QTM steps seems a common feature of many larger SMMs as well as some SCM systems.[8a,b,21,22]

The determination of an effective energy barrier to magnetization relaxation was accomplished by collecting plots of magnetization versus time decay in the temperature range 0.04−1 K for **1**. The measurements provide data on the rate of magnetization relaxation ($1/\tau$) versus T, where τ is the relaxation time. These data are plotted as τ versus $1/T$ in Figure 7, on the basis of the Arrhenius relationship of eq 3, where $1/\tau_0$ is the pre-exponential factor, U_{eff} is the mean

$$1/\tau = (1/\tau_0)\exp(-U_{\text{eff}}/kT) \qquad (3)$$

effective barrier to relaxation, and k is the Boltzmann constant. The best fit (dashed line) of the data gave $\tau_0 = 1.2 \times 10^{-7}$ s and $U_{\text{eff}} = 7.5$ K. The obtained barrier to relaxation is small, which is consistent with the observation of the hysteresis loops only at low temperatures. Also, the effective energy barrier U_{eff} is markedly smaller than the expected value (48.5 K) calculated from $U = S^2|D|$ for **1**, which is the maximum for the molecule.[21] This decrease may be related to the admixture of excited spin states. Thus, it is clear that complex **1** is a true SMM. Low-temperature magnetic measurements for **2**−**5** have not been carried out due to the limitation of our SQUID instrument; however, the structural similarity of **1**−**5** and the available magnetic data for **2**−**5** suggest that complexes **2**−**5** may similarly behave as SMMs.

TGA measurement shows that **1** fully loses its seven hydration water molecules above 120 °C (Figure S15, Supporting Information) and decomposes above 250 °C. The dehydrated sample of **1** was prepared by heating the sample at 150 °C for 2 h, which was subject to magnetic measurements. The temperature dependence and the field dependence of magnetization of the anhydrous sample show similarity to those of **1** (Figure S16, Supporting Information), indicating that the intermolecular magnetic coupling is mainly dipolar. Moreover, the removal of the crystallization water molecules did not ruin the backbone of the Mn_6Fe_6 wheels.

Magnetic Properties of 6. Variable-temperature magnetic susceptibilities of complex **6** were measured in the range 2−300 K, as shown in Figure 8 in the form of $\chi_m T - T$. The room-temperature $\chi_m T$ value is 7.0 emu K mol^{-1}, slightly larger than the expected spin-only value (6.75 emu K mol^{-1}) for the noninteracting $Mn^{III}_2Fe^{III}_2$ system with $g = 2.00$. On lowering the temperature, the $\chi_m T$ value of **6** gradually increases, reaches a maximum value of 8.10 emu K mol^{-1} at 10 K, and then sharply decreases to 4.45 emu K mol^{-1} at 2 K. The tendency of $\chi_m T$ confirms the presence of overall ferromagnetic interactions in this complex.

According to the crystallographic description, the magnetic susceptibility of **6** can be fitted by the following Hamiltonian:

$$\hat{H} = -J(s_1S_2 + S_2s_3 + s_3S_4) + g\beta S_z^T H - zJ'\langle S_z^T\rangle S_z^T \qquad (4)$$

where $(s, S) = (1/2, 2)$, $S_z^T = S_z + s_z$, J represents the magnetic coupling between Mn(III) and Fe(III) via a cyanide bridge, neglecting the bond angle difference of Mn−N≡C, and zJ' represents the intermolecular interaction.

The final results of the fitting procedure in the temperature range 2−300 K are shown as a solid line in Figure 8, and the fitted values are $J = 4.3$ K, $g = 2.0$ cm^{-1}, and $zJ' = -0.15$ cm^{-1}. To prove that the origin of the decrease of the

(20) Wernsdorfer, W. *Adv. Chem. Phys.* **2001**, *118*, 99−190.
(21) Brechin, E. K.; Boskovic, C.; Wernsdorfer, W.; Yoo, J.; Yamaguchi, A.; Sañudo, E. C.; Concolino, T. R.; Rheingold, A. L.; Ishimoto, H.; Hendrickson, D. N.; Christou, G. *J. Am. Chem. Soc.* **2002**, *124*, 9710−9711.
(22) Toma, L. M.; Lescouëzec, R.; Pasán, J.; Vaissermann, V.; Cano, J.; Carrasco, R.; Wernsdorfer, W.; Lloret, F.; Julve, M. *J. Am. Chem. Soc.* **2006**, *128*, 4842−4853. Ferbinteanu, M.; Miyasaka, H.; Wernsdorfer, W.; Nakata, K.; Sugiura, K.-i.; Yamashita, M.; Coulon, C.; Clerac, R. *J. Am. Chem. Soc.* **2005**, *127*, 3090−3099. Mishra, A.; Wernsdorfer, W.; Abboud, K. A.; Christou, G. *J. Am. Chem. Soc.* **2004**, *126*, 15648−15649.

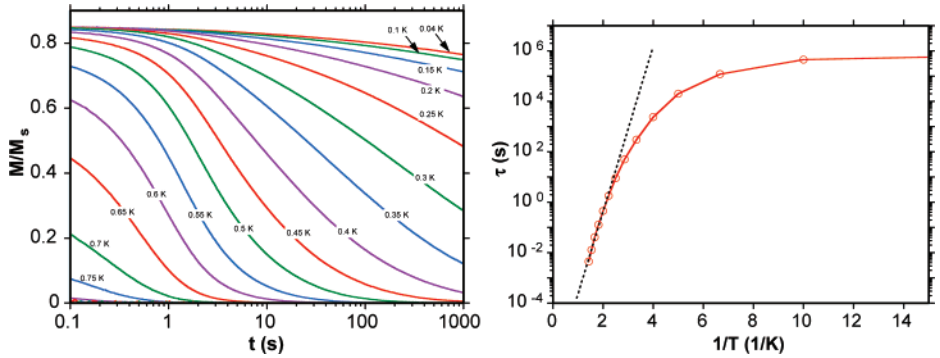

Figure 7. Magnetization relaxation and relaxation time $\tau \approx T^{-1}$ of **1**.

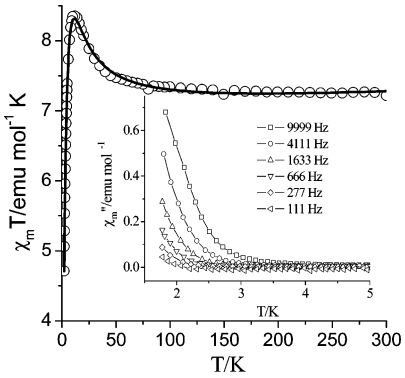

Figure 8. Temperature dependence of $\chi_m T$ for complex **6**. The line represents the best fit in the temperature range 2−300 K. Inset: out-of-phase ac magnetic susceptibilities of **6** measured under zero dc magnetic field.

susceptibility data below 10 K is mainly due to the intermolecular interactions, different simulations were carried out (a) for different values of the zJ' parameter and (b) for different values of the single-ion anisotropy of Mn(III) (incorporating in eq 4 the *SDS* term). The magnetic model shows great sensitivity to the intermolecular interaction in contrast with the zero-field splitting parameter of the Mn(III) ion that influences the low-temperature susceptibility data only for large and unrealistic D values (Figure S17, Supporting Information).

Assuming an $S = 5$ ground state, least-squares fitting of M versus H/T data for complex **6** affords $D = -0.42$ cm^{-1}, $E = 0$, $g = 1.8$, and $zJ' = -2(1) \times 10^{-2}$ cm^{-1} (Figure S18, Supporting Information). The fit reveals the negative character of the D parameter, while there is an important intertetramer interaction due to the hydrogen-bonding interactions, in agreement with the fit results of the $\chi_m T$ vs T curve.

Alternating-current magnetic measurements display obvious frequency-dependent χ_m'' signals below about 3.0 K (inset of Figure 8), indicating that the slow magnetization relaxation behavior occurs in **6** consistent with the direct-current magnetization data.

Conclusion

We have shown that the appropriate substitution groups in bpb^{2-} favor the formation of cyclic molecular structures. This research sheds light on the formation mechanism of cyanide-bridged cyclic complexes. Although the size of the molecular wheel is not that large (ca. 20 Å in diameter), the strategy raised here might be applied to the synthesis of other metallomacrocycles, and will thus enrich the metallomacrocycle family if successful. Magnetic investigations show that ferromagnetic coupling between adjacent metal ions is present, giving rise to an $S = 15$ high-spin ground state for the wheel compounds. Low-temperature magnetic measurements suggest that these wheel complexes form a new family of single-molecule magnets. However, albeit they have a high spin ground state, the blocking temperatures for the present SMMs are low partly because of the presence of weak intramolecular magnetic coupling and small magnetic anisotropic $|D|$ parameters.[13] To enlarge the energy barrier and increase the blocking temperature, it is desirable that the ground state is well separated from the excited spin states.[14] Therefore, the synthesis of strongly coupled Mn(III)−Fe(III) clusters is the next aim that is under way in our laboratory.

Experimental Section

Materials and Synthesis. All the starting chemicals were of AR grade and used as received. H_2bpmb, H_2bpClb, and H_2bpdmb were prepared by the literature methods.[23] K[Fe(bpmb)(CN)$_2$], K[Fe(bpClb)(CN)$_2$], and K[Fe(bpdmb)(CN)$_2$] have been synthesized according to literature procedures for K[Fe(bpb)(CN)$_2$].[24] The precursors [Mn(salen)]ClO$_4$, [Mn(5-Cl(salpn))]ClO$_4$, and [Mn(5-Br(salpn))]ClO$_4$ were synthesized according to a conventional procedure for [Mn(Schiff base)]ClO$_4$ complexes.[25] The synthesis and general characterization of complex **1** have been described elsewhere.[16]

Caution! *KCN is hypertoxic and hazardous. Perchlorate salts of metal complexes with organic ligands are potentially explosive. They should be handled in small quantities with care.*

[Fe(bpClb)(CN)$_2$]$_6$[Mn(salen)]$_6$·4H$_2$O·2CH$_3$OH (2) and [Fe(bpdmb)(CN)$_2$]$_6$[Mn(salen)]$_6$·10H$_2$O·5CH$_3$OH (3). Mn(salen)ClO$_4$ (42.0 mg, 0.1 mmol) was dissolved in 6 mL of a MeOH/MeCN mixture (1/1, v/v). K[Fe(bpClb)(CN)$_2$] (50.0 mg, 0.1 mmol) or K[Fe(bpdmb)(CN)$_2$] (49.5 mg, 0.1 mmol) dissolved in 5 mL of MeOH/H$_2$O (4/1, v/v) was carefully added to the former solution,

(23) Barnes, D. J.; Chapman, R. L.; Vagg, R. S.; Watton, E. C. *J. Chem. Eng. Data* **1978**, *23*, 349−350.
(24) (a) Ray, M.; Mukherjee, R.; Richardson, J. F.; Buchanan, R. M. *J. Chem. Soc., Dalton Trans.* **1993**, 2451−2457. (b) Dutta, S. K.; Beckmann, U.; Bill, E.; Weyhermuller, T.; Wieghardt, K. *Inorg. Chem.* **2000**, *39*, 3355−3364.
(25) Przychodzeń, P.; Lewinski, K.; Balanda, M.; Pełka, R.; Rams, M.; Wasiutynshi, T.; Guyard-Duhayon, C.; Sieklucka, B. *Inorg. Chem.* **2004**, *43*, 2967−2974.

and the mixture was immediately filtered and then left to stand undisturbed for 3 days at room temperature to yield uniform well-shaped dark brown single crystals suited for X-ray diffraction. Both **2** and **3** are reproducible with a high yield (ca. 60%). Anal. Calcd for $C_{218}H_{162}Fe_6Mn_6Cl_6N_{48}O_{30}$ (**2**): C, 44.42; H, 3.39; N, 13.97. Found: C, 44.05; H, 3.52; N, 13.65. Main IR bands (cm^{-1}): ν(C≡N), 2122m; ν(C═O), 1622vs. Anal. Calcd for $C_{233}H_{220}Fe_6Mn_6N_{48}O_{39}$ (**3**): C, 56.18; H, 4.45; N, 13.50. Found: C, 55.62; H, 4.78; N, 13.22. Main IR bands (cm^{-1}): ν(C≡N), 2121m; ν(C═O), 1619vs.

$[Fe(bpmb)(CN)_2]_6[Mn(5\text{-}Br(salpn))]_6\cdot 24H_2O\cdot 8CH_3CN$ (4). Regular hexagonal prismatic single crystals of **4** were obtained at room temperature by the slow diffusion of a dark green MeOH/H_2O (4/1, v/v) solution (5 mL) of K[Fe(bpmb)$(CN)_2$] (48.0 mg, 0.1 mmol) into a red-brown MeOH/MeCN (1/1, v/v) solution (5 mL) of [Mn(5-Br(salpn))]ClO_4 (51.6 mg, 0.1 mol) for about two weeks. Yield: 65%. Anal. Calcd for $C_{244}H_{210}Fe_6Mn_6Br_{12}N_{56}O_{36}$ (**4**): C, 46.21; H, 3.72; N, 12.37. Found: C, 45.87; H, 3.70; N, 11.94. Main IR bands (cm^{-1}): ν(C≡N), 2121m; ν(C═O), 1620vs.

$[Fe(bpmb)(CN)_2]_6[Mn(5\text{-}Cl(salpn))]_6\cdot 25H_2O\cdot 5CH_3CN$ (5) and $[Mn(5\text{-}Cl(salpn))]_2[Fe(bpmb)(CN)_2]_2\cdot 3H_2O\cdot CH_3CN$ (6). Two kinds of dark brown single crystals with different shapes, a regular hexagonal prism (**5**) and a rhombic block (**6**), appeared and were separated manually by the same procedure as for complex **4**. Yield: ca. 30% for **5** and 20% for **6**. Anal. Calcd for $C_{238}H_{227}Fe_6Mn_6Cl_{12}N_{53}O_{49}$ (**5**): C, 50.12; H, 4.01; N, 13.01. Found: C, 50.48; H, 3.85; N, 12.79. Main IR bands (cm^{-1}): ν(C≡N), 2120m; ν(C═O), 1618vs. Anal. Calcd for $C_{78}H_{66}Fe_2Mn_2Cl_4N_{17}O_{11}$ (**6**): C, 52.61; H, 3.74; N, 13.37. Found: C, 52.36; H, 3.96; N, 13.02. Main IR bands (cm^{-1}): ν(C≡N), 2123m; ν(C═O), 1620vs.

Physical Measurements. Elemental analyses (C, H, N) were carried out with an Elementar Vario EL analyzer. IR spectra were performed on a Nicolet Magna-IR 750 spectrometer in the 4000−650 cm^{-1} region. TGA measurement of **1** was performed in the temperature range 50−400 °C under nitrogen on a Universal V2.6D TA instrument. The room-temperature powder XRD analyses for **2**−**6** were performed over the angular range $5° < 2\theta < 40°$ with a 0.02° step on a Bruker D8-Discover high-resolution diffractometer with a Cu Kα source (λ = 1.5406 Å). Temperature- and field-dependent magnetic susceptibility measurements were carried out on a Quantum Design MPMS SQUID magnetometer from 2 to 300 K. The ac magnetic measurements were on a MagLab 2000 magnetometer with polycrystalline samples at frequencies ranging from 111 to 9999 Hz with an ac field amplitude of 3 G and no dc magnetic field applied. Magnetization measurements on a single crystal of **1** were performed with an array of micro-SQUIDs. This magnetometer works in the temperature range 0.04−7 K and in fields of up to 0.8 T with sweeping rates as high as 0.28 T/s. The experimental susceptibilities were corrected for the diamagnetism of the constituent atoms (Pascal's tables).

Single-crystal X-ray data of **2**−**6** were collected on a Rigaku R-AXIS RAPID IP diffractometer. The structures were solved by direct method SHELXS-97 and refined by full-matrix least-squares (SHELXL-97) on F^2. Hydrogen atoms were added geometrically and refined using a riding model. Some chloro groups from ligands $bpClb^{2-}$ in complex **2** experience disorder over two positions. The methyl group from $bpmb^{2-}$ in complexes **4** and **5** also experience disorder. The crystal data are summarized in Table 1.

CCDC 633509 (**2**) to CCDC 633513 (**6**) contain the supplementary crystallographic data for this paper. These data can be obtained free of charge at http://www.ccdc.cam.ac.uk/deposit.

Monte Carlo (MC) simulations are powerful numerical tools for high-precision studies of many-body systems, in both the classical and quantum regimes. Especially near second-order phase transitions, where physical length scales diverge, it is essential to simulate large systems, which has become possible due to significant algorithmic advances within the last 15 years.

In this paper QMC studies were carried out to simulate the magnetic behavior of the wheel compounds **1**−**5**,[26] on the basis of the stochastic series expansion (SSE) algorithm,[27] a generalization of Handscomb's algorithm[28] for the Heisenberg model. While in the original implementation[27] local MC updates were used, Sandvik later developed a cluster update, called the operator-loop update for the SSE representation,[29] which allows for nonlocal changes of MC configurations. Within this SSE approach one can efficiently simulate models for which the world line loop algorithm suffers from slowing. The reason for using the QMC method instead of the classical Monte Carlo (CMC) method is the quantum nature of the LS-Fe(III) ion (S = 1/2).

The QMC calculations are based on the ALPS (algorithms and libraries for physical simulations) project.[30] For each site were performed 5×10^6 Monte Carlo steps, and 10% of them were discarded as the initial transient stage.

The magnetic susceptibility of compound **6** was fit using the MAGPACK[31] program employed with a nonlinear least-squares curve-fitting program, DSTEPIT.[32] The magnetization data of compounds **1**−**6** were fit by using the same curve-fitting program and a homemade Fortran program that sets up a 961 × 961 or 121 × 121 spin Hamiltonian matrix for compounds **1**−**5** and **6**, respectively, for the determination of the energy levels by matrix diagonalization with the EISPACK[33] subroutines.

Acknowledgment. This work was supported by the Fok Ying Tong Education Foundation and the Natural Science Foundation of China (Grant 20671055). H.-Z.K. thanks Prof. Yadong Li for helpful discussions.

Supporting Information Available: Plots of molecular structures for complexes **3** and **5**, ac magnetic susceptibility measured in zero dc applied magnetic field for **2**−**6**, magnetization vs H/T plots for **2**, **3**, and **5** in the ranges 2−4 K and 10−50 kG, simulations of the magnetic susceptibility for various values of intermolecular interaction or the single-ion anisotropy of Mn(III) for **6**, temperature dependence of $\chi_m T$ for **1** and the dehydrated sample **1** − $7H_2O$, field dependence of magnetization of **1** and **1** − $7H_2O$ at 2 K, and TGA curve of **1**.

IC700528A

(26) A Monte Carlo study was carried out instead of the usual diagonalization procedure of the full Hamiltonian matrix using the ITO (irreducible tensor operators) method because of the large dimension of Hilbert's space (10^6).
(27) (a) Sandvik, A. W.; Kurkijarvi, J. *Phys. Rev.* **1991**, *B43*, 5950−5961. (b) Sandvik, A. W. *J. Phys.* **1992**, *A25*, 3667.
(28) Handscomb, D. C. *Proc. Cambridge Philos. Soc*. **1962**, *58*, 594; **1964**, *60*, 115.
(29) Sandvik, A. W. *Phys. Rev.* **1999**, *B59*, R14157−R14160.
(30) Alet, F.; et al. (ALPS collaboration). *J. Phys. Soc. Jpn., Suppl*. **2005**, *74*, 30.
(31) Borrás-Almenar, J. J.; Clemente-Juan, J. M.; Coronado, E.; Tsukerblat, B. S. *J. Comput. Chem.* **2001**, *22*, 985−991.
(32) Program 66, Quantum Chemistry Program Exchange, Indiana University, Bloomington, IN.
(33) Garbow, B. S. Applied Mathematics Division, Argonne National Laboratory, Argonne, IL.